Adsorption (2011) 17: 325–335
DOI 10.1007/s10450-010-9314-2

# A method for the determination of accessible surface area, pore volume, pore size and its volume distribution for homogeneous pores of different shapes

**D.D. Do · L.F. Herrera · D. Nicholson**

Received: 23 February 2010 / Accepted: 21 December 2010 / Published online: 4 January 2011


**Abstract** We develop a novel method to determine the accessible pore volume, the accessible pore size and its distribution for pores having homogeneous surfaces but taking an arbitrary shape. The *accessible* pore volume is essentially the volume space that is accessible to the centre of an adsorbate molecule, while the *accessible* pore size is defined by the largest sphere that can be accommodated in the accessible space. The size of this sphere depends on the point in the accessible volume that we select. The accessible pore size is therefore, a local variable and this means that even a geometrically simple pore can possess many sizes. Each local accessible pore size is associated with a local accessible pore volume and the relationship between this pore volume and pore size is called the accessible pore size distribution. In this paper, we illustrate this methodology with a number of model pores ranging from simple to complex geometry and present the analytical accessible pore size distribution.

**Keywords** Pore size distribution · Surface area · Homogeneous pores · Accessible volume

## 1 Introduction

Characterization of porous media has been an important topic for many decades and it is receiving even greater attention from scientists and engineers working with porous solids (Gregg and Sing 1982; Rouquerol et al. 1999; Do 1998). This is because of the development of advanced porous solids whose pore structures do not have any regular or well defined shape, and therefore the use of classical methods (Kaneko et al. 2002; Do et al. 2007; Birkett and Do 2007; Sing et al. 1985; Rouquerol et al. 1994; Kaneko 1994; Kaneko et al. 1998; Thommes et al. 2002; Thommes 2004; Do et al. 2008b; Jagiello and Betz 2008; Olivier and Occelli 2004) becomes inapplicable because they assume that pores have either slit or cylindrical shape. Typical examples of this are porous alumina, silica gel and cubic cage structures of metal organic frameworks (MOF) (Li et al. 1999; Rowsell and Yaghi 2004). The importance of characterization is reflected in the two major meetings in this area, Characterization of Porous Solids (COPS) and Characterization of Porous Materials Workshop, whose theme is dedicated purely to characterization.

Even when the atomistic configuration of a solid is known, it is desirable to obtain the pore volume distribution. For this reason, some authors have proposed different computational methods to calculate the Pore Size Distribution (PSD) for a well-defined solid, such as those developed by Torquato (Torquato et al. 1990; Torquato and Avellaneda 1991; Lu and Torquato 1993), Gubbins (Gelb and Gubbins 1999; Kendall and Gubbins 2000; Pikunic et al. 2003; Bhattacharya and Gubbins 2006) and Do (Herrera et al. 2008; Do et al. 2008a; Birkett et al. 2009). All these methods calculate the pore size by fitting a sphere into the cavities of the pores, however each method uses a different scheme to calculate the position of the sphere in the pore. For example Gelb and Gubbins (1999) defined the volume based on the Connolly surface while Do and co-workers used the surface traced at zero potential energy (Do et al. 2008a). Because all these methods use a sphere as a yardstick to measure the size of the pore, the location of the sphere's centre is the most important matter because an incorrect location results in the misrepresentation of the PSD. Since different methods have different theoretical approaches to the determination of the pore size, they can give different answers. Here we present

D.D. Do (✉) · L.F. Herrera · D. Nicholson
School of Chemical Engineering, University of Queensland,
St. Lucia, Qld 4072, Australia
e-mail: d.d.do@uq.edu.au

analytical solutions of the PSD for some ideal pores, calculated using classical geometry based on the accessible pore volume concept presented by Do (Do and Do 2007). We will call this PSD the Accessible Pore Size Distribution (APSD) because of its relation to the accessible volume. The APSDs will be used to justify an improved Monte Carlo integration (MCI) scheme compared with the previous one presented in earlier work (Do et al. 2008a).

## 2 Theory

### 2.1 Accessible pore volume

The accessible pore volume is defined as the volume accessible to the centre of mass (centre of geometry can also be used) of a particle at zero loading (Do and Do 2007). For solids whose atomistic configurations are known, this can be determined by MCI (Do et al. 2008a). For the purpose of characterization, it is appropriate that we choose noble gases because they are inert, spherical and non-polar; argon is the most logical choice. Nitrogen is also a good candidate as it is the most widely used probe, but its adsorption is somewhat specific because its quadrupole favours strong electrostatic adsorption sites, such as high affinity functional groups. Furthermore, because it is non-spherical, it can adopt different orientations, which noble gases cannot.

The procedure for determining the accessible pore volume is as follows. We insert a particle at a random position in the simulation box and calculate its potential energy with the solid by summing all pairwise potential energies between this test particle and all solid atoms, and then remove it from the box (to simulate the zero loading condition). If the solid-fluid potential is either zero or negative, that insertion is a success. If the fluid particle has a shape (for example nitrogen), we perform this step as follows. First, we insert the centre of mass of a particle at a random position and give it a random orientation. If the solid-potential energy is non-positive, we count that insertion as a success; otherwise, we choose another orientation and if it becomes non-positive, the insertion is a success. If after multiple different orientations the solid-fluid potential remains positive, the insertion is a failure. This insertion process is repeated many times with uniform random distribution (i.e. every point within the simulation box has an equal chance of being selected). This means that we sample the space of the simulation box with equal probability, and if the fraction of success is $f$, then the accessible volume is simply $f$ times the volume of the simulation box (i.e. sampling volume), $V_{\text{acc}} = f V_{\text{box}}$.

### 2.2 Definition of pore size

For pores with an arbitrary shape, one could define the characteristic pore size as $4V/S$, where $V$ is the void volume and $S$ is the surface area. Unfortunately, this choice is not suitable for pores having void space with wide variation in size. We must recognize that pore size is a local variable and therefore a pore can possess many sizes to reflect the different sizes in different parts of the pore. To avoid the orientation issue with the way one would measure the pore size, we propose to use a sphere as the yardstick and the size of this sphere will give us the measure of the pore size. The problem now is simply to find a way to locate this sphere and its size. This size is defined as the pore size and since the sphere is enclosed within the accessible pore space, we will call this *accessible pore size*.

### 2.3 Model pores

Because the aim is to calculate the PSD *analytically*, we have used model pores with homogeneous surfaces. This type of surface is commonly adopted in simulation such as those using the Steele 10-4-3 potential model (Steele 1973) or the Crowell potential (Crowell 1954) for flat surfaces, or the Tjatjopoulos et al. (1988) equation for cylindrical pores.

#### *2.3.1 Infinitely long and homogeneous slit and cylindrical pores*

We start with the simplest pore: an infinitely long slit pore. Clearly, there is only one accessible pore size as shown in Fig. 1a, and its associated accessible pore volume is the space bounded by the dashed line located where the solid-fluid potential of a spherical probe particle is zero. The largest sphere (and the only sphere) that fits in this pore is

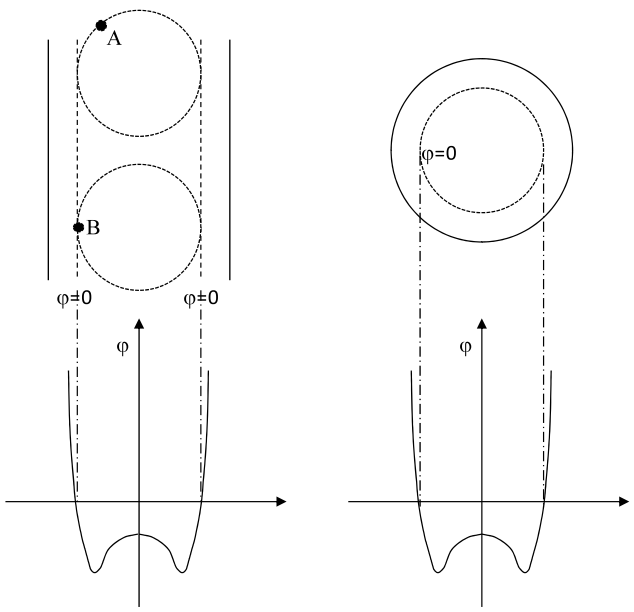


**Fig. 1** (**a**) Infinitely long, homogeneous slit pore; (**b**) Infinitely long, homogeneous cylindrical pore. The *dashed line* is the boundary of zero solid-fluid potential energy

shown in Fig. 1a as the dotted line. A molecular probe placed anywhere in that sphere will have a non-positive solid-fluid potential. Indeed, for any point chosen at random in the accessible volume (i.e. the volume bounded by the dashed lines) we can find the largest sphere that encloses that point or has it on its surface. For example, with the point A in Fig. 1a in the accessible volume, the largest sphere is the one that passes through that point. Likewise if the point is chosen on the boundary of the accessible volume (point B) we also find the largest sphere as shown in Fig. 1a. So, for this simple geometrical pore, we have only one pore size, as expected.

Similarly, for an infinitely long structureless cylindrical pore (Fig. 1b) we have again only one accessible pore size and its associated pore volume is the space bounded by the dashed line. The largest sphere that fits in this pore is shown as a dotted line (superimposed exactly on the dashed line). A molecular probe placed anywhere in that sphere will have non-positive solid-fluid potential. Thus, for a homogeneous long slit or cylinder, the determination of the analytical accessible pore size and accessible pore volume is simple.

### 2.3.2 *Pores with corners*

Real pores are not infinitely long like the ones that we have discussed in the last section. We now turn to pores with corners and determine the pore size of corners.

*2.3.2.1 Conical pores* Consider a cone-typed pore as shown in Fig. 2 (solid line). The included angle of the cone is $2\alpha$. Let the accessible void volume be the space bounded by the boundary shown as a dashed line in this figure. The largest sphere that can access the cone is shown as a dotted line. It resides at the right side of the cone with its surface tangential to the boundary of the accessible volume. Let the diameter of this largest hemi-sphere be $D_1$. We shall define the pore size as follows: any points residing on the surface of this $D_1$-hemisphere will have a pore size $D_1$. Any points residing inside the hemisphere will have pore sizes greater than $D_1$ and any point enclosed by the cone and this hemisphere will have a pore size smaller than $D_1$.

From what has been said, the accessible volume that has pore sizes smaller than $D$ is simply the volume in the tip of the cone bounded by the boundary of the accessible volume and the surface of the $D$-sphere (shown as shaded sphere in Fig. 2). Mathematically the cumulative accessible volume up to size $D$ is:

$$V(D) = \frac{\pi D^3}{24} \frac{(1-\sin\alpha)^2}{\sin\alpha} \tag{1}$$

Similarly, the cumulative accessible volume for pores smaller that $D'$ is also given by (1), with $D$ replaced by $D'$. Therefore, the accessible pore volume having sizes falling between $D$ and $D'$ is $(D' > D)$

$$V(D < x < D') = \frac{\pi(D'^3 - D^3)}{24} \frac{(1-\sin\alpha)^2}{\sin\alpha} \tag{2}$$

where $x$ is the pore size. This is the required formula to determine the accessible pore volume. We denote the relationship between the accessible pore volume and the accessible pore size as the accessible pore size distribution. The change of this pore volume with the pore size $D$ is the derivative of $V$ with respect to $D$:

$$\frac{dV}{dD} = \frac{\pi}{8} \frac{(1-\sin\alpha)^2}{\sin\alpha} D^2 \tag{3}$$

Figure 3 shows the APSD of the cone. The APSD is presented as the scaled cumulative accessible volume versus pore size. The APSD starts from zero accessible pore size that is simply the size at the tip of the accessible volume (point A in Fig. 2), then the cumulative volume increases monotonically with the pore size as the power of three. It

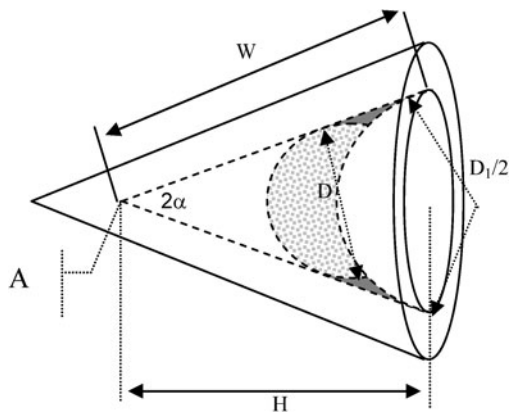


**Fig. 2** One-dimensional cone-type corner

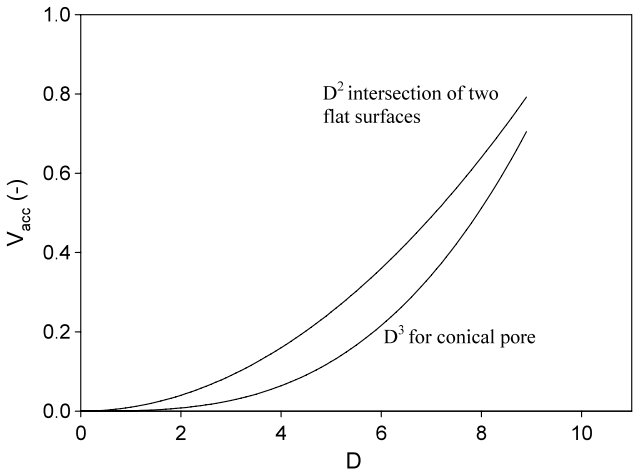


**Fig. 3** Cumulative APSD for a cone pore and the intersection of two flat surfaces

should be stressed that zero accessible size of a pore is possible and its corresponding physical pore size is one below which the adsorbate cannot enter. Detailed discussion of zero accessible pore size has been given in Do et al. (2008a).

*2.3.2.2 Pores formed by two walls* Next, we consider a pore formed by the intersection of two surfaces as shown in Fig. 4. The figure does not show the physical pore walls, but rather it shows only the two surfaces of zero potential that bound the accessible volume. The accessible pore volume corresponding to pore sizes smaller than $D$ is simply the volume bounded by the two boundary surfaces and the surface of a cylinder (which is tangential to the two boundary surfaces) having a diameter $D$ because of the infinite extent in the $z$-direction (Fig. 4). This volume is shown as a dotted region in Fig. 4. Let the length of the pore be $W$, then the shaded volume is given by:

$$V(D) = \frac{D^2 W}{4}\left[\frac{\cos\alpha}{\sin\alpha} - \left(\frac{\pi}{2} - \alpha\right)\right] \tag{4}$$

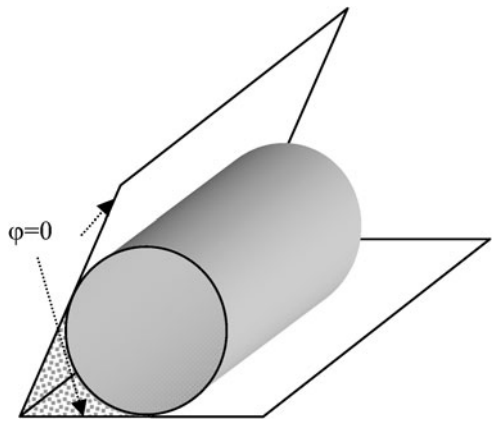


**Fig. 4** Pore created by the intersection of two flat surfaces

where $\alpha$ is half of the angle between the two surfaces. Equation (4) is the cumulative volume for pores having sizes less than $D$, and we see that cumulative volume increases with the square of the pore size instead of the power 3 as in the conical pores. From (4) we can derive a working formula for the accessible volume having sizes falling between $D$ and $D'$ as follows:

$$V(D < x < D') = \frac{W}{4}\left[\frac{\cos\alpha}{\sin\alpha} - \left(\frac{\pi}{2} - \alpha\right)\right](D'^2 - D^2) \tag{5}$$

The change of the pore volume with respect to the pore size for this 2D-pore is

$$\frac{dV}{dD} = \frac{W}{2}\left[\frac{\cos\alpha}{\sin\alpha} - \left(\frac{\pi}{2} - \alpha\right)\right]D \tag{6}$$

Thus, the change of the pore volume behaves linearly with pore size, in contrast to the square of $D$ in the conical pore.

A representation of the APSD is shown in Fig. 3. This APSD has a parabolic behaviour. This trend is a characteristic of this pore and distinguishes the two dimensional pore from the cone type pore.

*2.3.2.3 Pore formed by three walls* Another class of pore is that formed by the intersection of three surfaces, such as the cubic pore shown in Fig. 5. The total accessible volume is the cube shown as solid line. The question now is that what are the sizes for this pore? The largest pore size is the size of the sphere (grey colour) that fits this cubic pore (i.e. this sphere is tangential to six surfaces of the cubic accessible volume). Let the diameter of this sphere be $D_{max}$. This sphere is defined as the one for which a molecular probe residing anywhere in this sphere has a non-positive solid-fluid potential. Of course, we also have the space near the eight corners to deal with. How do we do this? Let us assume that we are interested in another pore size, say $D$ ($< D_{max}$). The sphere of size $D$ touches the three surfaces and is shown in Fig. 5b as the cross-hatched region. We call this sphere the

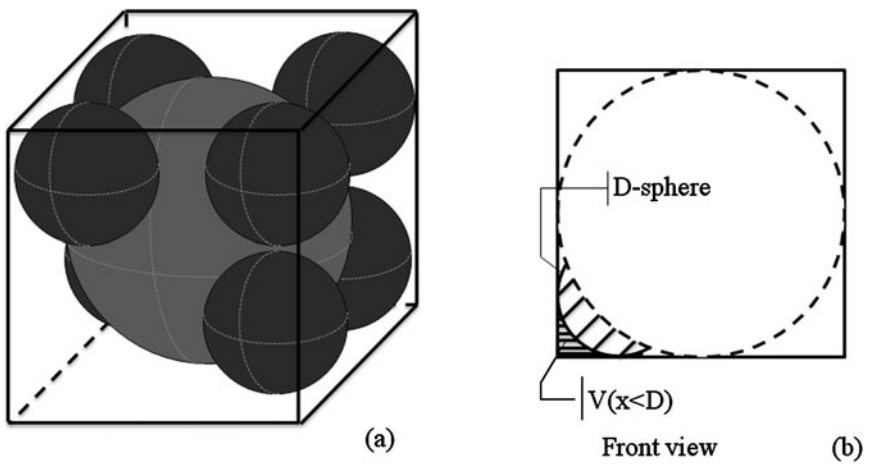


**Fig. 5** The schematic diagram of a pore created by the intersection of three orthogonal flat surfaces (**a**) and its front view (**b**)

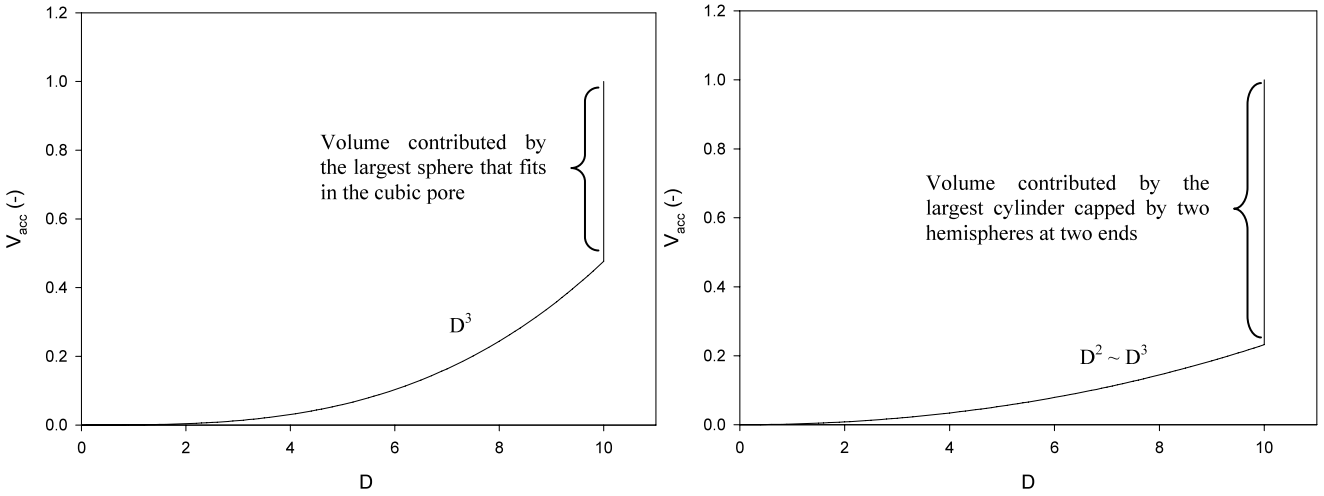


**Fig. 6** Cumulative APSD for a (LHS) cubic pore and a (RHS) rectangular pore. The initial $D^3$ behaviour of the cubic pore is typical for 3D corner, including the conical pore, while the rectangular pore has an initial part behaving between $D^2$ and $D^3$

$D$-sphere. The region marked by the horizontal line is the accessible volume that has sizes smaller than $D$. This volume is simply eight times (because we have eight corners in this cubic pore) the difference between the volume of the cube having linear dimension of $D/2$ and the one-eighth of the $D$-sphere, that is:

$$V(x < D) = \left(1 - \frac{\pi}{6}\right) D^3 \tag{7}$$

The contribution from one corner is one-eight of that given in (7). Therefore, the working formula for the accessible volume having sizes falling between $D$ and $D'$ is:

$$V(D < x < D') = \left(1 - \frac{\pi}{6}\right)(D'^3 - D^3) \tag{8a}$$

and the accessible volume having size $D_{\max}$ is:

$$V(D_{\max}) = \frac{\pi}{6} D_{\max}^3 \tag{8b}$$

The agreement of (7) and (8) and the total accessible volume can be checked by summing the cumulative volume of the accessible volume having sizes less than $D_{\max}$ plus the volume of the $D_{\max}$-sphere, which is $D_{\max}^3$.

The rate of change of the accessible volume with pore size is proportional to the pore size, $dV/dD = 3(1 - \pi/6)D^2$. This has the same dependence on $D$ as the conical pore.

A cumulative APSD for this pore is shown in Fig. 6. The cumulative APSD shows that for pore sizes less than cube's size, the cumulative accessible volume increases with pore size as the power of three. This behaviour is similar to that observed earlier for the cone shaped pore. When the pore size is equal to the cube's size, the cumulative APSD shows a sudden jump due to the large contribution from the maximum pore size. This abrupt change in volume is the main difference between the APSD of this corner and that of the cone shaped pore.

An extension of the cubic pore is a rectangular pore as shown in Fig. 7. The largest sphere is the sphere shown as dotted line. It is tangential to the four or five surfaces of the accessible volume (rather than six in the case of cubic pore). Let the diameter of this sphere be $D_{\max}$. The accessible pore volume associated with this pore size is not just the volume of this sphere, but rather the grey volume as shown in the figure. This volume has a central cylindrical part with two hemi-spheres at the two ends, and its volume is the accessible pore volume associated with the pore size $D_{\max}$. The pore sizes for the eight corners are determined in the same manner as for the cubic pore, while the pore sizes along the four long edges are obtained in the same manner as the pore created by the intersection of two walls in the previous section. The working formula for the accessible pore size distribution in a pore of length $L$ having size $D_{\max}$ is:

$$V(D_{\max}) = \frac{\pi}{6} D_{\max}^3 + \frac{\pi D_{\max}^2}{4}(L - D_{\max}) \tag{9a}$$

and the accessible volume having sizes falling between $D$ and $D'$ is given by:

$$\begin{aligned} &V(D < x < D') \\ &= \left(1 - \frac{\pi}{6}\right)(D'^3 - D^3) \\ &\quad + \left(1 - \frac{\pi}{4}\right)(L - D_{\max})(D'^2 - D^2) \end{aligned} \tag{9b}$$

The first term on the RHS of the above equation is contributed by the eight corners (Fig. 7b) while the second term

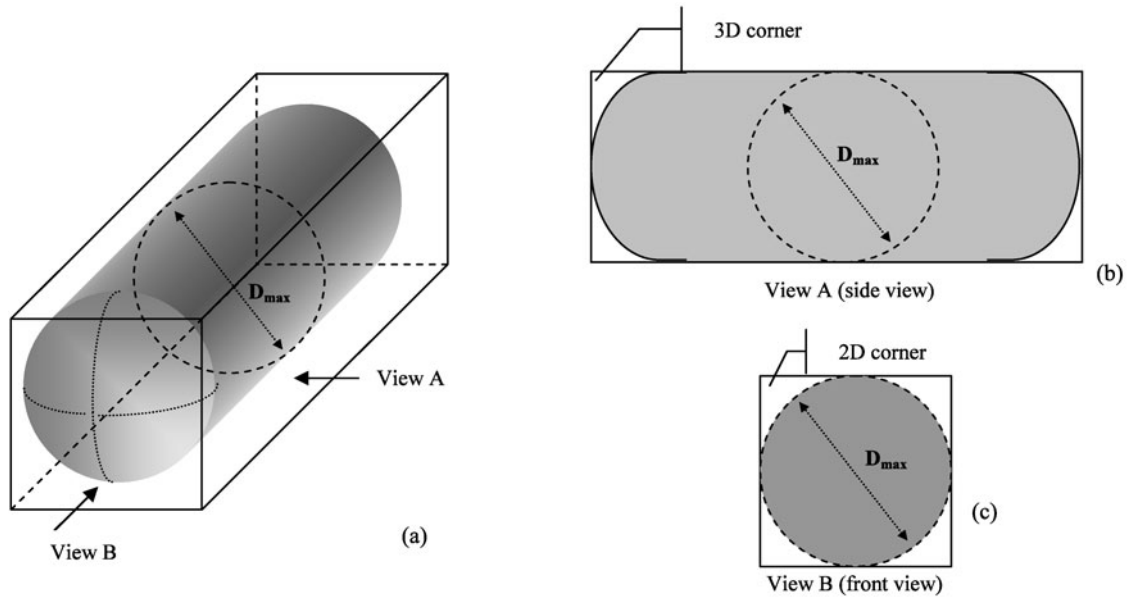


**Fig. 7** A rectangular pore. 3D representation (**a**), side view (**b**) and front view (**c**)

comes from the four edges (Fig. 7c) along the pore. To check these equations, we take the sum of all accessible volumes which should equal the total accessible volume, $L D_{\max}^2$. The accessible volume contributed by all corners is

$$V(0 < D < D_{\max}) = \left(1 - \frac{\pi}{6}\right) D_{\max}^3 + \left(1 - \frac{\pi}{4}\right)(L - D_{\max}) D_{\max}^2$$

and the sum of this volume plus the volume associated with $D_{\max}$ (see (9a)) is indeed equal to the total accessible volume.

The cumulative volume in (9b) has a pore size dependence of $D^2$ and $D^3$, typical for the 2D-corner and the 3D-corner, respectively. The APSD of the rectangular pore is shown in Fig. 6. This behaviour is similar to the cubic pore. The differences are; the greater contribution of the volume associated with the maximum pore size $D_{\max}$, and the behaviour of the volume versus pore size ($D < D_{\max}$) has two contributions. One is due to the eight corners at the two ends of the pore (increase with $D$ according to $D^3$), and the four edges along the pore length (increase with $D$ according to $D^2$).

*2.3.2.4 Carbon nanotube bundles* We consider two configurations of carbon nanotube bundles: Triangular (Fig. 8a) and square (Fig. 8b). The gray region this figure is the total accessible volume for these configurations. Let $D_0$ be the size of the carbon nanotube and $2\Delta$ be the distance between the centres of the adjacent nanotubes. The maximum pore size ($D_{\max}$) for these two configurations are given by

$$D_{\max} = \begin{cases} \frac{4\Delta}{\sqrt{3}} - D_0 & \text{for a triangular bundle} \\ 2\sqrt{2}\Delta - D_0 & \text{for a square bundle} \end{cases} \tag{10a}$$

and the pore volume corresponding to this pore size is

$$V(D_{\max}) = \frac{\pi D_{\max}^2 W}{4} \tag{10b}$$

where $W$ is the length of the carbon nanotube.

If the distance between the two cylinders is greater than the diameter of the cylinder, the minimum pore size is

$$D_{\min} = 2(\Delta - D_0/2) \tag{10c}$$

For the space between the carbon nanotubes, we have the following equation for the accessible pore volume as a function of accessible pore size:

$$\frac{V}{W} = \begin{cases} A + B & \text{for } D_{\min} \le D < D^* \\ A & \text{for } D^* < D < D_{\max} \end{cases} \tag{10d}$$

where the parameter $D^*$ is the critical diameter of the sphere which is tangent to two adjacent nanotubes and the plane passing through the central lines of these nanotubes (Fig. 8c). The parameters $A$ and $B$ are given by

$$A = \frac{2\gamma\Delta R}{R + R_0} - \frac{\pi R_0^2}{2} + (R_0^2 - R)(\sin\beta\cos\beta + \beta)$$
$$B = \frac{\pi R^2}{2} - \gamma\sqrt{R^2 - \gamma^2} - R^2 \sin^{-1}\left(\frac{\gamma}{R}\right) \tag{10e}$$

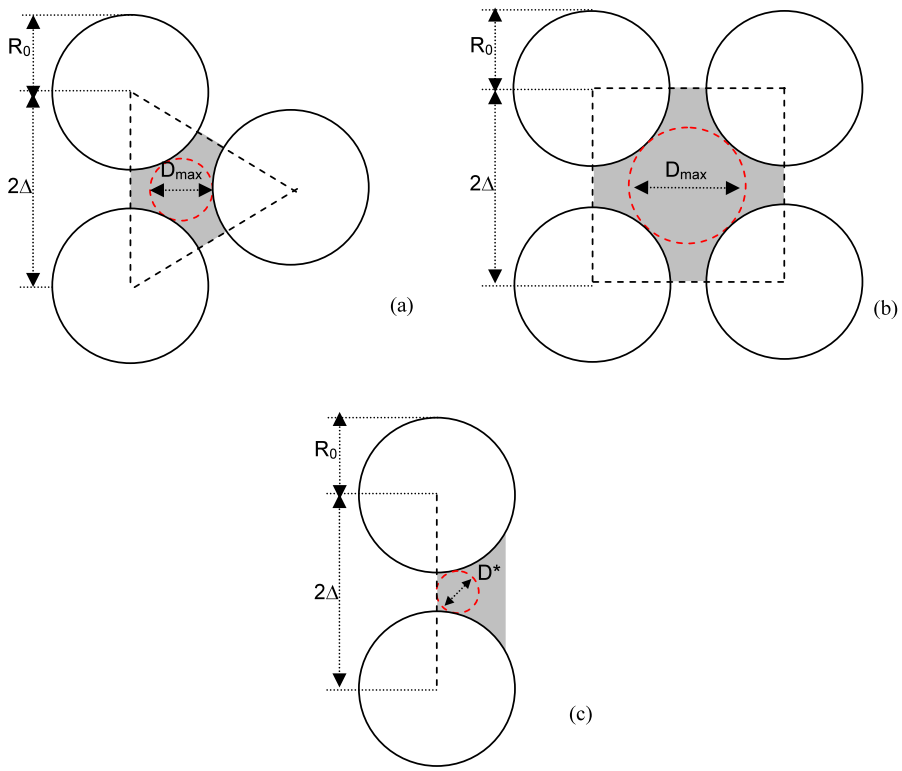


**Fig. 8** The void space formed between carbon nanotubes (**a**) triangular and (**b**) square bundle. Representation of the parameter $D^*$ (**c**)

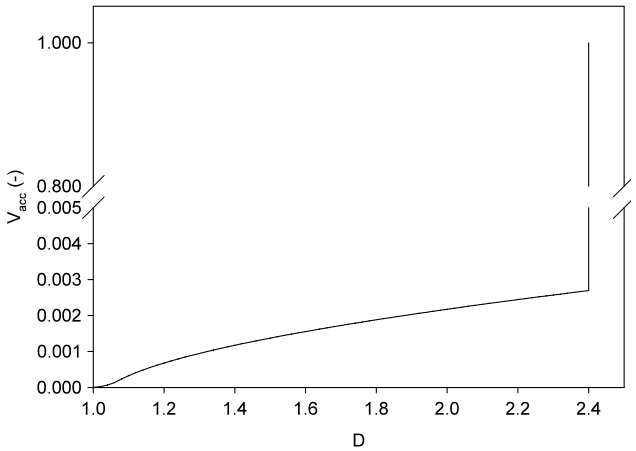


**Fig. 9** Cumulative APSD for a tube bundle

and

$$D = 2R; \qquad D^* = \frac{(\Delta^2 - R_0^2)}{R_0}; \qquad \gamma = \sqrt{(R + R_0)^2 - \Delta^2}; \qquad \sin\beta = \Delta/(R + R_0). \tag{10f}$$

The main features of the APSD for a tube bundle are shown in Fig. 9. The APSD shows an increasing cumulative accessible volume with pore size for pores smaller than $D_{\max}$ and then a sudden jump of the volume for a pore size equal to $D_{\max}$. This sudden jump is again due to the contribution of this maximum pore size. The APSD of the tube bundle can be distinguished from the one of the cube or rectangular pores because of the convex concavity in the APSD for small pores while the other two show a concave shape.

### 2.3.3 *Cubic framework (idealized metal organic framework)*

Finally, we consider an idealized model for metal organic framework. This idealized model is a hollow cube constructed with 12 lines of equal length $2\Delta$ (Fig. 10a). The sphere of maximum size that can fit in that hollow cubic structure has a diameter of $2\Delta\sqrt{2}$. This sphere protrudes from the six sides of the cube as shown in Fig. 10b.

The volume of the sphere confined within the cubic structure is the difference between the volume of the sphere and 6 times the volume of the portion of the sphere protruding beyond the surface. It is

$$V(D_{\max}) = 2\pi\left(5 - \frac{8\sqrt{2}}{3}\right)\Delta^3 \tag{11}$$

where $D_{\max} = 2\Delta\sqrt{2}$. Now we consider a sphere of radius $D$ smaller than $D_{\max}$ that fits into one of the corners of the cubic framework. This sphere touches the three lines and the centre of this sphere is at a distance of $D/2\sqrt{2}$ from the surfaces $xy$, $xz$ and $yz$ and protrudes from these surfaces. The volume that has pore sizes less than $D(= 2R)$ is the difference between the volume bounded by the cube that has

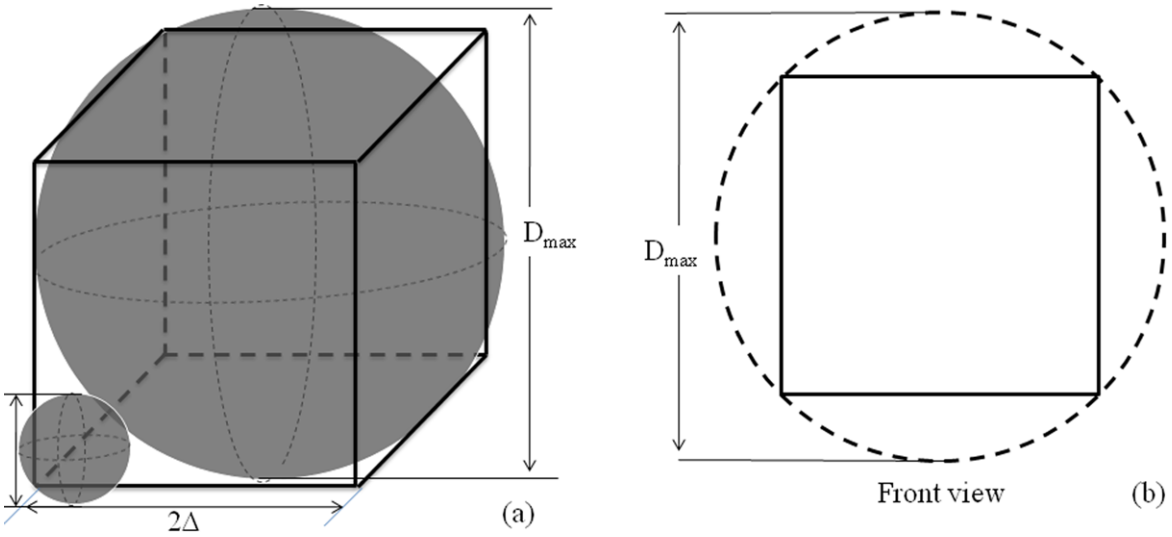


**Fig. 10** 3D representation of an idealized hollow cubic structure (**a**). The largest sphere shows the largest pore size $D_{\max}$ while the other shows a pore size of $D$. Front view of the idealized hollow cubic structure (**b**)

the origin and the center of the $R$-sphere as two of the eight vertices and the portion of the $D$-sphere that overlaps with the cube. This volume is

$$V(x < D) = 8\left(\frac{\pi}{3} + \frac{1}{2\sqrt{2}} - \frac{5\pi}{8\sqrt{2}}\right)R^3 \tag{12}$$

for $D$ less than $D_{\max}$. Thus, the cumulative volume for pore sizes up to $D$ follows a $D^3$-dependence. The factor 8 in the RHS of the above equation is because we have eight such corners in the framework. To prove that we have derived the correct equation for the cumulative volume we show that the cumulative volume for the corners at $D_{\max}$ plus the volume at $D_{\max}$ (see (11)) must yield the cubic volume of the framework. Substituting $R$ by $R_{\max} = \Delta\sqrt{2}$ into (12) and adding the result to (11) indeed gives the correct volume of the framework, which is $8\Delta^3$. Thus the working formula for the pore size distribution is

$$V(x < D') - V(x < D)$$

the accessible pore volume having pore sizes falling between $D$ and $D'$.

The APSD of the idealized metal organic framework shows an increasing accessible pore volume with pore size according to the power of three, for small pores. Then, there is a sudden jump due to the contribution of the largest pore size ($D_{\max}$). This is similar to the APSD of the cubic pore.

## 3 Implications of the analytical APSD

As stated initially, the main reason to calculate the analytical solutions of the APSD for some ideal pores is to establish a reference point to improve the Monte Carlo integration (MCI) method proposed by Do and co-workers (Do et al. 2008a). In this section, we present the main implications of the analytical APSDs for developing a MCI method.

### 3.1 Method to sample the accessible volume

In the literature, there are different methods to calculate the PSD by using a sphere as a yardstick. Some methods calculate the volume by gridding it and then selecting different points in the grid at which to place the sphere (Gelb and Gubbins 1999; Kendall and Gubbins 2000; Pikunic et al. 2003). As the APSD is based on the accessible volume, it is desirable that the volume calculated follows the same procedure as the accessible volume (Do and Do 2006). The method does not require a grid and all the coordinate points $(x, y, z)$ have the same probability of being selected in a MC integration method. The procedure is as follows.

A single particle is inserted at a random position in the simulation box, and then its potential energy with the solid is calculated by summing all pairwise potential energies between this test particle and all solid atoms. If the solid–fluid potential is either zero or negative, that insertion is a success, otherwise is a failure. This insertion process is repeated many times with uniform random distribution (i.e. every point within the simulation box has an equal chance of being used for the particle insertion. This means that we sample the space of the simulation box with equal probability), and if the fraction of success is $f$ then the accessible volume is simply $f$ times the volume of the simulation box, $V_{\text{acc}} = f V_{\text{box}}$. This method can also be used for polyatomic molecules (Do et al. 2008a).

### 3.2 Surface area

From the analytical APSD, it is seen that the surfaces of the solid is defined as the boundary of zero solid-fluid potential energy between the test sphere (at zero loading) and the solid (see Fig. 1 as an example). This surface is consistent with the accessible volume and can also be calculated with MCI by using the method proposed by Do and coworkers (Herrera et al. 2010). This is called the accessible surface and differs from other PSD methods (Gelb and Gubbins 1999; Kendall and Gubbins 2000; Pikunic et al. 2003; Bhattacharya and Gubbins 2006) that use the Connolly surface (Connolly 1983).

### 3.3 Calculating the pore size

This is done in the same manner as in the determination of the total accessible pore volume, but this time we need to determine the local accessible pore size for each particular successful insertion.

When a successful insertion has been located (at point $A$ say), the next step is to re-locate the centre of a sphere until a position is found for which the largest sphere that can be accommodated in the pore, encloses the point $A$. Any points selected in this sphere, including its surface, have non-positive solid-fluid potential energy. We use the solid atoms positions to calculate the path to the final position where the sphere defining the pore size is located. That is the center of the sphere is moved away from the two or three closest solid atoms (the selection of the two or three solid atoms depends on the complexity of the solid configuration and it is part of the MCI method).

We now give examples of the trajectory of the sphere for some of the ideal models presented previously.

#### *3.3.1 Infinite long and homogeneous slit and cylindrical pores*

The first pore to be considered is the slit pore. After an insertion point with a non-positive potential $A$ is chosen, we search for the two closest points on the solid surface from this insertion point. Let these points be $S^{(I)}$ and $S^{(II)}$, with the first point being the closest one to the insertion point $A$. We shall present an iterative procedure to search for the largest sphere such that the following two criteria are satisfied:

(C1) This sphere encloses the insertion point $A$
(C2) Any point in this sphere has a non-positive solid-fluid potential.

We proceed our iteration process by assigning the insertion point $A$ and its associated two closest points on the surface as $A_1$, $S_1^{(I)}$ and $S_1^{(II)}$, with the subscript to denote the iteration number. We use the convention that the first point on the solid surface, $S_1^{(I)}$, is the closest point to $A_1$. The algorithm is described below.

Algorithm:

1. Once $A_1$ has been chosen and its two associated closest points on the solid surface are found, the next point in the iteration process depends on the distances $|A_1 S_1^{(I)}|$ and $|A_1 S_1^{(II)}|$. If one is shorter, we will choose a new point $A_2$ along the direction of the shorter vector $\overrightarrow{S_1^{(I)} A_1}$ by an increment $\delta$; otherwise if these two distances are equal we then move along the combined vector $\overrightarrow{S_1^{(I)} A_1} + \overrightarrow{S_1^{(II)} A_1}$ again with an increment $\delta$. If this combined vector is zero, we move along the direction normal to the vector $\overrightarrow{S_1^{(I)} A_1}$ to the new point $A_2$.
2. Once $A_2$ has been found, we again find the two closest points on the surface, denoted them as $S_2^{(I)}$ and $S_2^{(II)}$. A sphere whose centre at $A_2$ is found such that the two criteria C1 and C2 are met.
3. We repeat the steps 1 and 2 until the criterion C1 is violated.
4. The size of the largest sphere in the whole iteration process is then taken to be the accessible pore size associated with the insertion point $A$.

Applying the above algorithm to the case of infinitely long and homogeneous slit pore, we insert a point $A$ into the pore space. This point $A$ has non-positive solid-fluid potential energy. This is the iteration 1 (Fig. 11a). Carrying the step 1 of the algorithm a number of times we will find the point $A_n$, at which the distances between this point and the two closest points on the surface are equal (Fig. 11b). Repeating the same step, we move along the direction normal to the vector $\overrightarrow{A_n S_n^{(I)}}$. This is done until we find the point $A_m$ such that sphere whose centre at this point will have the insertion point $A$ on its surface, and the size of this sphere is the accessible pore size associated with that insertion point $A$.

If the insertion is carried out several times ($M$) and since the simulation box is sampled with a uniform distribution (i.e. each point in the sampling volume has an equal chance of being selected), the volume associated for each insertion is $V/M$, where $V$ is the volume of the simulation box. For this infinitely long homogeneous slit pore every successful insertion gives the same pore size, and therefore the volume associated with this pore size is simply $f \times V/M$, where $f$ is the fraction of successful insertion.

#### *3.3.2 Conical pores*

The most complex pore needed to demonstrate the path that the sphere follows to find the pore size is the conical pore.

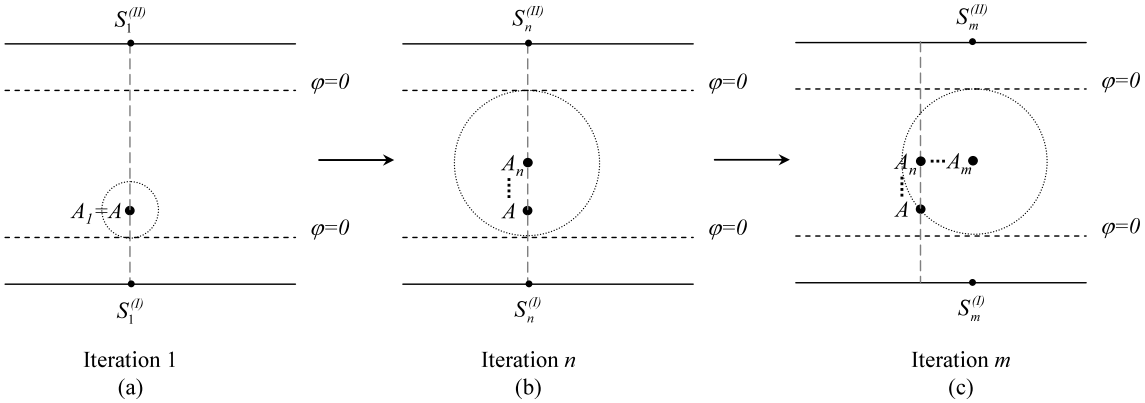


**Fig. 11** Monte Carlo iteration scheme for a slit pore

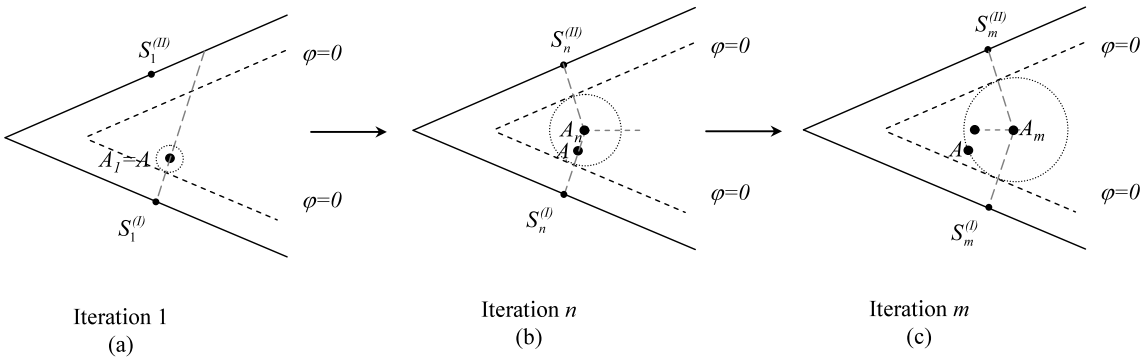


**Fig. 12** Monte Carlo iteration scheme for a conical pore

This is because it is the most straightforward configuration to understand and because the method is repeated exactly in the same way for more complex configurations.

Consider the conical pore shown in Fig. 2. The algorithm that was presented earlier for the slit pore works equally well for any pores, including this conical pore. We illustrate the iterations graphically in Fig. 12 for the conical pore.

To calculate the APSD, the method suggested above is followed for several successful insertion points. Then accessible volume associated with the accessible pore size $R_j$ is calculated by $V_{\text{acc},j} = f_j \times \text{V}_{\text{box}}$, where $f_j$ is the fraction of successful insertions of pore size $j$. The total accessible volume can be calculate by $V_{\text{acc}} = \sum V_{\text{acc},j}$. The plot of the differential volume $V_{\text{acc},j}$ versus $R_j$ is the accessible pore size distribution.

## 4 Conclusions

We have presented in this paper a definition of pore size for pores whose shapes do not conform to the well-defined geometries such as slit, cylinder or sphere. Using this definition, we derive analytical solutions of the APSD for a number of pore structures. This is the first time that analytical solutions of pore size distributions, calculated in this manner, have been presented in the literature. The different configurations of pore structures yield different fingerprints, that could be used to distinguish one configuration from another. The significant outcome of this work is that the accessible pore size and accessible volume are defined in an unambiguous manner. Additionally, the analytical pore size distributions presented here is used to outline a modified MCI method to calculate the APSD. The results of the modified MCI method for complex solids will be presented in a future publication.

**Acknowledgement** This work is supported by the Australian Research Council.

## References

Bhattacharya, S., Gubbins, K.E.: Fast method for computing pore size distributions of model materials. Langmuir **22**, 6 (2006)

Birkett, G.R., Do, D.D.: On the physical adsorption of gases on carbon materials from molecular simulation. Adsorption 407–424 (2007)

Birkett, G.R., Herrera, L.F., Do, D.D.: The properties of virtual solids using Monte Carlo integration and their value to the nanoscientist. In: 8th International Symposium on the Characterisation of Porous Solids, Edinburgh, 10–13th June (2009)

Connolly, M.L.: Analytical molecular surface calculation. J. Appl. Crystallogr. **16**, 548–558 (1983)

Crowell, A.D.: Approximate method of evaluating lattice sums of $r^{-n}$ for graphite. J. Chem. Phys. **22**(8), 1397–1399 (1954)

Do, D.D.: Adsorption Analysis: Equilibria and Kinetics. Imperial College Press, London (1998)

Do, D.D., Do, H.D.: Modeling of adsorption on nongraphitized carbon surface: GCMC simulation studies and comparison with experimental data. J. Phys. Chem. B **110**(35), 17531–17538 (2006)

Do, D.D., Do, H.D.: Appropriate volumes for adsorption isotherm studies: the absolute void volume, accessible pore volume and enclosing particle volume. J. Colloid Interface Sci. **316**(2), 317–330 (2007)

Do, D.D., Birkett, G., Do, H.D.: Adsorption of simple and complex fluids on non-graphitized carbon black and activated carbon—transition from sub-critical to supercritical adsorption and a new method to determine pore size distribution of activated carbon. Plenary Lecture at Carbon meeting, Seattle, US, June (2007)

Do, D.D., Herrera, L.F., Do, H.D.: A new method to determine pore size and its volume distribution of porous solids having known atomistic configuration. J. Colloid Interface Sci. **328**, 110–119 (2008a)

Do, D.D., Ustinov, E.A., Do, H.D.: Porous texture characterization from gas-solid adsorption. In: Bottani, E.J., Tascon, J.M.D. (eds.) Adsorption by Carbon, pp. 239–271. Elsevier, Amsterdam (2008b)

Gelb, L.D., Gubbins, K.E.: Pore size distribution in porous glasses: a computer simulation study. Langmuir **15**(2), 305–308 (1999)

Gregg, S.J., Sing, K.S.W.: Adsorption, surface Area and Porosity. Academic Press, New York (1982)

Herrera, L.F., Do, D.D., Birkett, G.R.: Characterization of virtual nanostructures through the use of Monte Carlo integration. In: Advanced Materials Research, pp. 275–278 (2008)

Herrera, L., Do, D.D., Nicholson, D.: A Monte Carlo integration method to determine accessible volume, accessible surface area and its fractal dimension. J. Colloid Interface Sci. **348**(2), 529–536 (2010)

Jagiello, J., Betz, W.: Characterization of pore structure of carbon molecular sieves using DFT analysis of Ar and H2 adsorption data. Microporous Mesoporous Mater. **108**(1–3), 117–122 (2008)

Kaneko, K.: Determination of pore size and pore size distribution, 1: adsorbents and catalysts. J. Membr. Sci. **96**(1–2), 59–89 (1994)

Kaneko, K., Ishii, C., Kanoh, H., Hanzawa, Y., Setoyama, N., Suzuki, T.: Characterization of porous carbons with high resolution a-analysis and low temperature magnetic susceptibility. Adv. Colloid Interface Sci. **76–77**, 295–320 (1998)

Kaneko, K., Ohba, T., Hattori, Y., Sunaga, M., Tanaka, H., Kanoh, H., Rodriguez-Reinoso, F., Unger, K.: Role of gas adsorption in nanopore characterization. In: Studies in Surface Science and Catalysis, pp. 11–18. Elsevier, Amsterdam (2002)

Kendall, T.T., Gubbins, K.E.: Modeling structural morphology of microporous carbons by reverse Monte Carlo. Langmuir **16**, 13 (2000)

Li, H., Eddaoudi, M., O'Keeffe, M., Yaghi, O.M.: Design and synthesis of an exceptionally stable and highly porous metal-organic framework. Nature **402**, 476–479 (1999)

Lu, B., Torquato, S.: Chord-length and free-path distribution functions for many-body systems. J. Chem. Phys. **98**(8), 6472–6482 (1993)

Olivier, J.P., Occelli, M.: An overview of physical adsorption methods for the characterization of finely divided and porous materials and their application to fluid cracking catalysts. In: Studies in Surface Science and Catalysis, pp. 1–33. Elsevier, Amsterdam (2004)

Pikunic, J., Clinard, C., Cohaut, N., Gubbins, K.E., Guet, J.M., Pellenq, R.J.M., Rannou, I., Rouzaud, J.N.: Structural modelling of porous carbons: constrained reverse Monte Carlo method. Langmuir **19**, 20 (2003)

Rouquerol, J., Avnir, D., Fairbridge, C.W., Everett, D.H., Haynes, J.H., Pernicone, N., Ramsay, J.D.F., Sing, K.S.W., Unger, K.K.: Recommendations for the characterization of porous solids. Pure Appl. Chem. **66**(8), 1739–1758 (1994)

Rouquerol, F., Rouquerol, J., Sing, K.: Adsorption by Powders and Porous Solids Principles, Methodology and Applications. Academic Press, New York (1999)

Rowsell, J.L.C., Yaghi, O.M.: Metal-organic frameworks: a new class of porous materials. Microporous Mesoporous Mater. **73**, 3–14 (2004)

Sing, K.S.W., Everett, D.H., Haul, R.A.W., Moscou, L., Pierotti, R.A., Rouquerol, J., Siemieniewska, T.: Reporting physisorption data for gas/solid systems with special reference to the determination of surface area and porosity (Recommendations 1984). Pure Appl. Chem. **57**(4), 603–619 (1985)

Steele, W.A.: Physical interaction of gases with crystalline solids. Surf. Sci. **36**(1), 317–352 (1973)

Thommes, M.: Physical adsorption characterization of ordered and amorphous mesoporous materials. In: Lu, G., Zhao, X.S. (eds.) Nanoporous Materials, Science & Engineering, pp. 317–364. Imperial College Press, London (2004)

Thommes, M., Köhn, R., Fröba, M., Aiello, R., Testa, F.: Characterization of mesoporous solids: pore condensation and sorption hysteresis phenomena in mesoporous molecular sieves. In: Studies in Surface Science and Catalysis, pp. 1695–1702. Elsevier, Amsterdam (2002)

Tjatjopoulos, G., Feke, D., Adin Mann, J.: Molecule micropore interaction potentials. J. Phys. Chem. **92**(13), 4006–4007 (1988)

Torquato, S., Avellaneda, M.: Diffusion and reaction in heterogeneous media: Pore size distribution, relaxation times, and mean survival time. J. Chem. Phys. **95**(9), 6477–6489 (1991)

Torquato, S., Lu, B., Rubinstein, J.: Nearest-neighbor distribution functions in many-body systems. Phys. Rev. A **41**(4), 2059 (1990)